Applied Catalysis B: Environmental 160–161 (2014) 692–700

Contents lists available at ScienceDirect

Applied Catalysis B: Environmental

journal homepage: www.elsevier.com/locate/apcatb

Sonophotocatalytic (42 kHz) degradation of Simazine in the presence of Au–TiO_2 nanocatalysts

Panneerselvam Sathishkumar[a,b,*], Ramalinga Viswanathan Mangalaraja[a,*], Héctor D. Mansilla[c], M.A. Gracia-Pinilla[d,e], Sambandam Anandan[f]

[a] Advanced Ceramics and Nanotechnology Laboratory, Department of Materials Engineering, Faculty of Engineering, University of Concepcion, Concepcion 407-0409, Chile
[b] Department of Chemistry, Periyar Maniammai University, Vallam, Thanjavur 613403, Tamil Nadu, India
[c] Faculty of Chemical Sciences, University of Concepcion, PO Box 160-C, Correo 3, Concepcion, Chile
[d] Universidad Autónoma de Nuevo León, Facultad de Ciencias Físico-Matemáticas, Av. Universidad, Cd. Universitaria, San Nicolás de los Garza, NL, Mexico
[e] Universidad Autónoma de Nuevo León, Centro de Investigación e Innovación en Desarrollo de Ingeniería y Tecnología, Avenida Alianza 101 Sur PIIT Monterrey, Apodaca 66600, NL, Mexico
[f] Nanomaterials and Solar Energy Conversion Lab, Department of Chemistry, National Institute of Technology, Trichy 620 015, India

ARTICLE INFO

Article history:
Received 12 April 2014
Received in revised form 27 May 2014
Accepted 17 June 2014
Available online 23 June 2014

Keywords:
42 kHz ultrasound
Sonophotocatalysis
Simazine
HPLC and ESI-MS analysis

ABSTRACT

The nano-size gold loaded visible light driven Au–TiO_2 nanophotocatalysts were synthesized using a commercial sonicator bath producing 42 kHz ultrasound. The X-ray diffraction (XRD), transmission electron microscopy (TEM) and high angle annular dark field (HAADF) scanning transmission electron microscopy (STEM) analyses revealed the gold nanoparticles incorporated in the TiO_2 resides at the surface of the nanocatalysts. An increased BET surface area was observed for the Au–TiO_2 when compared with the bare TiO_2 which gave the first notation that the gold nanoparticles modified the physicochemical characteristics of the TiO_2. The RAMAN spectrum shows the shift by ~5 cm^{-1} at 639 cm^{-1} which indicated that the loaded gold nanoparticles were loaded on the surface of TiO_2 nanoparticles and thus confirms that the gold nanoparticles readily accepts the electronic charges created during the photoexcitation of Au–TiO_2 nanocatalysts. The Simazine (triazine based pesticide) was taken as the model pollutant to evaluate its sonocatalytic, photocatalytic and sonophotocatalytic degradation in the presence of TiO_2 and Au–TiO_2 nanocatalysts. The first order kinetics was observed for the Simazine degradation. The observed rate constants indicate that the order of degradation of Simazine was, sonophotocatalysis > sonocatalysis > photocatalysis. The additive effect was observed for the Au–TiO_2 assisted sonophotocatalytic degradation of Simazine. A 1.65 and 1.38 fold enhanced mineralization was achieved for the sonophotocatalytic degradation of Simazine when compared with the photocatalytic and sonocatalytic processes. The intermediates produced during the mineralization of Simazine were analyzed using ESI-MS analysis and based on that a suitable mechanism has been proposed.

1. Introduction

To increase the agricultural productivity, pesticides have been widely applied in its different forms such as insecticides, herbicides and fungicides. However the custom of pesticides in the agricultural lands for the last five decades caused the notorious impact to the environment and its related hazardous effects to the living organisms [1–5]. Among the various pest control agents used in the agriculture, Simazine (2-chloro-4,6-bis(ethylamino)-*s*-triazine) (Fig. 1) is a triazine based synthetic pesticide which is the second largest one used to control the pest in the agricultural lands since 1956 [2,6–8]. The maximum solubility of Simazine in water is 5 mg/L [9], the excessive addition (or the undissolved quantity) of the Simazine in the agricultural lands was dissolved during the rainy season and the running water carries the Simazine from one end to the other end which tends to cause the environmental aquatic pollution. Arias-Estévez et al. [10] found that only a minor fraction of Simazine (0.1%) is effective for the pest killing action and

* Corresponding authors at: University of Concepcion, Department of Materials Engineering, Advanced Ceramics and Nanotechnology Laboratory, Edmundo Larenas 270, Concepcion, Chile. Tel.: +56 41 2207389; fax: +56 41 2203391.
E-mail addresses: sathish_panner2001@yahoo.com, sathishpanner2001@gmail.com (P. Sathishkumar), mangal@udec.cl (R.V. Mangalaraja).

http://dx.doi.org/10.1016/j.apcatb.2014.06.027
0926-3373/

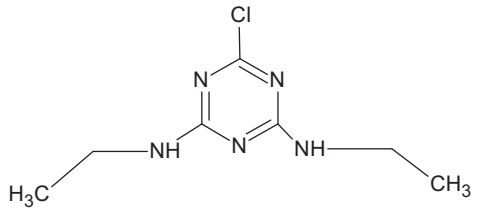

Fig. 1. Molecular structure of Simazine.

the remaining quantity enters into the environment which causes the soil, air and water pollution. Moreover, triazine based pesticides have shown its reduced effect in the growth as well as the reproduction of zooplankton species [11]. Therefore, triazine based pesticides essentially need to be completely mineralized to avoid the hazardous effects engendered by its presence in the environment.

In order to completely mineralize the Simazine, some of the techniques such as adsorption [12], ozonation [13,14], Fenton's oxidation [7], UV photolysis [14] and biodegradation [15] have been practiced in the past and among the various technologies available for the mineralization of Simazine, TiO_2 photocatalysis have shown moderately enhanced degradation when compared with the other methodologies. However, the disadvantages like adsorption of the substrate and its derivatives on the surface of the solid support, rate of migration of electronic charges produced at the surface of nanocatalysts during photocatalysis need to be improved to attain the enhanced rate of mineralization. Hence, the combination of photocatalysis with other advanced oxidation processes (AOPs) was expected to increase the rate of degradation of Simazine when compared to the effect of single-handed AOPs. In this study, we combined a 42 kHz low intensity ultrasound producing commercial sonicator with the visible light assisted photocatalysis technique to improve the mineralization of Simazine. Concurrently, it is expected that the combination of sonophotocatalysis can reduce the operating cost of the mineralization process and the development of visible light responsive photocatalysts can further reduce the operating cost required for the sonophotocatalytic mineralization of organic contaminants.

Titanium dioxide is an extensively studied material for the energy and environmental applications [16] and it could not be photo-excited by the wavelength greater than 387 nm which limits the application of sunlight as an energy source for the excitation of TiO_2. The loading of noble metals on the surface of TiO_2 can enhance the optical as well as catalytic properties [17–19]. The surface plasmon resonance (SPR) emitted by the noble metal nanoparticles can enhance the localized electric field in the contiguous metal and/or semiconductor particles which allows to facilitate the formation of electronic charges (e^- and h^+) [20,21]. On the other hand, the difference in the work function (φ) of the gold nanoparticles (φ_{Au} = 5.1 eV) and TiO_2 (φ_{TiO_2} = 4.2 eV) further decreases the rate of recombination of electronic charges which are created during the photoexcitation of Au–TiO_2 [22]. The loaded gold nanoparticles can reduce the band gap of TiO_2 from 3.2 eV and enhance the visible light response of the nanocatalysts. Hence the loading of gold nanoparticles on the surface of TiO_2 enhances the physical separation of the electronic charges and thereby increasing the resulting quantum yield of the catalytic processes. Based on the previous studies and the necessity to evaluate the sonophotocatalytic efficiency of the gold loaded TiO_2 nanocatalysts, in this study, we synthesized the Au–TiO_2 by a simple low frequency ultrasound (42 kHz) assisted sonochemical process and the resulted nanocatalysts were employed to evaluate the sonocatalytic, photocatalytic, and sonophotocatalytic degradation of Simazine.

2. Experimental

2.1. Materials and methods

Titanium dioxide (Aeroxide®P25) and Chloroauric acid trihydrate ($HAuCl_4 \cdot 3H_2O$) were purchased from Sigma-Aldrich and used as the starting materials for the preparation of Au and Au–TiO_2 nanoparticles. Simazine ($C_7H_{12}N_5Cl$) was received from Sigma-Aldrich and used without further purification. Unless otherwise specified, all reagents used were of analytical grade and the solutions were prepared using double distilled water. The crystallite size of the synthesized nanoparticles was calculated from the X-ray diffraction data (Philips PW1710 diffractometer, Cu $K\alpha$ radiation, Holland) using Scherrer equation. Surface morphology and microstructure of the nanocatalysts were analyzed by transmission electron microscopy (TEM, FEI TITAN G2 80-300) operated at 300 KeV. Diffuse reflectance UV–vis spectra of the nanocatalysts were recorded using a Shimadzu 2550 spectrophotometer equipped with an integrating sphere accessory employing $BaSO_4$ as reference material. Raman spectra were recorded using a Dilor LabRam-1B spectrometer, operating at a resolution of 1 cm^{-1}. The surface area, pore volume and pore diameter of the nanocatalysts were measured with the assistance of Flowsorb II 2300 of Micrometrics, Inc.

The kinetics of Simazine degradation was followed using a HPLC (Perkin Elmer) equipped with a PDA detector (model Flexar), the Brownlee analytical C18 column (5 um, 150 × 4.6 mm) was employed for the HPLC analysis. The UV detection was operated at 222 nm. The mobile phase composition was H_2O/acetonitrile with a ratio of 40/60. The injection volume was 20 μL and the flow rate was 1 mL/min. The retention time for Simazine was 5 min under these HPLC conditions. A fresh stock solution of Simazine was prepared before the experiments. Simazine calibration curve was prepared for concentrations between 0.0015 and 5 mg/L with a correlation coefficient of R^2 = 0.9998. The calibration curve for Simazine was constructed using the peak areas of the standard samples under the same conditions as that of the experimental samples. The total organic carbon (TOC) for all the samples was analyzed by direct injection of the filtered sample solutions into a TOC analyzer (Vario TOC cube, Cientec Instrumentos South America). Prior to the analysis, the instrument was calibrated with potassium hydrogen phthalate. TOC_0 is the TOC measured after the equilibrium adsorption of the dye on the nanocatalysts surface and TOC obtained at various irradiation times is denoted as TOC_t. The degradation products were analyzed by using LC/MSD Trap VL (G2445C VL) electrospray ionization mass spectrometry (ESI-MS^n) system coupled with Agilent Chem Station (version B.01.03) data-processing station. The mass spectra data were processed with the Agilent LC/MS Trap software (version 5.3).The instrument was calibrated using the automatic tuning procedure with respect to the parent compound as the standard. The mass range scanned was m/z 50–1200 and several spectra were obtained across each chromatographic peak.

2.2. Preparation of nanocatalysts

2.2.1. Preparation of gold nanoparticles

The gold nanoparticles and gold loaded TiO_2 was prepared according the procedure reported by Anandan and Ashokkumar [23] with a slight modification in the synthesis procedure as follows: the gold precursor solution (5.25×10^{-4} M) was prepared along with 0.1 M isopropanol followed by the addition of 0.1 wt% of polyethylene glycol under the vigorous stirring and then it is transferred into a 42 kHz ultrasound producing commercial bath type sonicator. The irradiation was continued up to 30 min, the samples were withdrawn at regular intervals during the irradiation for the

UV–vis spectroscopic analysis. The synthesized nanoparticles were characterized using various analytical techniques to confirm the formation of the gold nanoparticles.

2.2.2. Preparation of Au–TiO_2 nanocatalysts

The gold precursor solution (5.25×10^{-4} M) along with 0.1 M isopropanol solution was stirred vigorously for 15 min and subsequently the titanium dioxide (1 g) was added, and then the suspension was irradiated for 30 min. The color of the suspension was changed from yellow to violet after the completion of 30 min sonication which we presumed that the entire precursor (Au^{3+}) was converted to gold nanoparticle (Au^0) and it was assumed that the above procedure yielded a gold loading of ~1 mol% on TiO_2.The nanocatalysts were gathered by filtration (0.45 μm Nylon filter membranes) until the pH of the solution reached 7. The solids were dried at 100 °C in a hot air-oven for 12 h followed by the calcination at 550 °C for 5 h in order to get pure nanocatalysts. Similarly, the bare TiO_2 was treated using the same methodology and calcined at 550 °C for comparison.

2.3. Photocatalysis and sonophotocatalysis

The Simazine solutions were freshly prepared by dissolving the appropriate amount (5 mg/L) of Simazine in 250 mL and filtered using a 0.2 μm polytetrafluoroethylene syringe filter (PTFE, Cole-Parmer, USA) in order to remove any undissolved Simazine. To optimize the concentration of the nanocatalysts for the enhanced degradation of Simazine, Au–TiO_2 was varied from 0.2 g/L to 3.0 g/L. The degradation of Simazine was studied under ambient atmospheric conditions and at natural solution pH (~6.0). In order to ensure the adsorption/desorption equilibrium, the Simazine/nanocatalyst slurry was stirred for 45 min in dark condition prior to irradiation. After that, the lamp and/or the sonicator were turned on and this was taken as "time zero" for the degradation reactions. The photocatalytic studies were performed using a light source (Cole-Parmer, USA) illuminating spectral range ≥ 420 nm with the intensity of incident irradiation = 100,000 ± 100 Lx measured by Lux meter (Cole-Parmer, USA). All the sonochemical reactions in this study were carried out by using a commercially available sonicator (8890, Cole-Parmer, USA) producing 42 kHz ultrasonic waves. The experimental setup and conditions used for photolysis, sonolysis, and sonophotolysis were identical. During the degradation studies, the target substance (Simazine) was sonicated in the presence and absence of nanocatalysts and visible light. The apparent kinetics of disappearance of the substrate (Simazine) was determined by following its concentration using HPLC analysis (PerkinElmer). Prior to the analysis, the nanocatalysts were separated from the suspension by using a 0.2 μm PTFE filter.

3. Results and discussion

3.1. Characterization of gold and gold loaded TiO_2 nanocatalysts

The formation of gold nanoparticles was monitored by UV–vis spectroscopic analysis and the characteristic changes during the synthesis of gold nanoparticles from the precursor solution are shown in Fig. 2. The formation of gold nanoparticles instigates after 3 min of irradiation of the precursor solution and the reaction was completed within 30 min under 42 kHz ultrasound. It is observed from the UV–vis spectroscopic analysis that the extended ultrasonic irradiation (<30 min) tends to decrease the surface plasmon resonance (SPR) absorption of the resulting gold nanoparticles [24] (data not shown).The observed decrease in the SPR absorption clearly indicates that the completion of gold nanoparticles formation. The inset of Fig. 2 shows the corresponding digital photograph

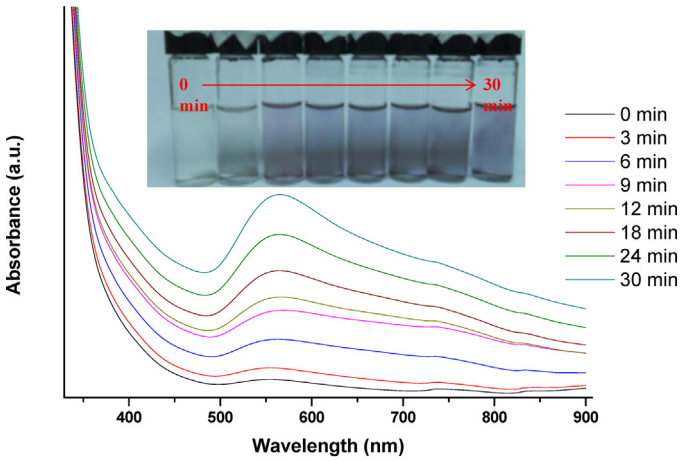

Fig. 2. UV–vis absorption spectra of sonochemically reduced Au nanoparticles at various time intervals and the inset shows the corresponding digital photographs.

of the gold nanoparticles withdrawn from its precursor solution at frequent intervals of ultrasonic irradiation. Fig. 3a and b shows the representative HRTEM images of the synthesized gold nanoparticles. The clear distribution of gold nanoparticles was noticed and the measured particle size was in the range from 2 to 5 nm (Fig. 3a). The lattice fringe distance calculated from Fig. 3b was 0.23 nm which is the clear indication of the formation of Au (1 1 1) crystal plane and was predominantly formed during the ultrasonic irradiation. The FFT pattern (Fig. 3c) demonstrated that the mixed phases was formed during the synthesis of gold nanoparticles, however, the crystal nature is conquered in the resulting gold nanoparticles.

The representative HRTEM images of Au–TiO_2 nanocatalysts are shown in Fig. 4. Fig. 4a and b reveals that the gold nanoparticles were tethered at the surface of the TiO_2 which confirms that the 42 kHz of ultrasonic irradiation kindled the adequate distribution of gold nanoparticles. Fig. 4c clearly indicates the existence of Au (1 1 1) and titanium dioxide (1 0 1) crystal planes in the synthesized Au–TiO_2 nanocatalysts which authenticate the fine distribution of gold nanoparticles on the surface of TiO_2. The average particle size of the Au–TiO_2 calculated from the HRTEM analysis was ~21 nm. The observed FFT pattern (Fig. 4d) for the Au–TiO_2 nanocatalysts additionally supports the formation of Au (1 1 1) during its synthesis. The EDAX analysis (Fig. 4e) further confirms the presence of gold and TiO_2 nanoparticles. The scanning transmission electron microscopy (STEM) with a high angle annular dark field (HAADF) analysis (Fig. 4f) of the Au–TiO_2 nanocatalysts indicates the loaded gold nanoparticles are distributed at the surface of the TiO_2 and the penetration of gold nanoparticles was not supported by the present experimental conditions. In addition, the presence of the gold nanoparticles at the TiO_2 surface could improve the separation of electronic charges during the visible light excitation of the Au–TiO_2 nanocatalysts.

The X-ray diffraction analysis of the synthesized nanocatalysts is shown in Fig. 5. The appearance of strong intense peak at $2\theta = 25.4^\circ$ corresponds to the (1 0 1) anatase phase that confirms its predominant in the TiO_2 and Au–TiO_2 nanocatalysts (JCPDS file no. 211272). However, the appearance of rutile peaks was also observed in the TiO_2 and Au–TiO_2 nanocatalysts at $2\theta = 27.6$ and 36.2 (JCPDS file no. 211276) which clearly indicate that the anatase-rutile ratio is not affected by the gold nanoparticles doping in TiO_2. The decrease in the intensity of Au–TiO_2 was observed when compared to the bare TiO_2 due to the loading of gold nanoparticles which affects the crystallinity of the resulting nanocatalysts. The XRD analysis of Au–TiO_2 may not be able to exhibit any specific diffraction peak for the existence of gold nanoparticles due to the low quantity of loading. The average crystallite size of Au–TiO_2 nanocatalysts calculated using

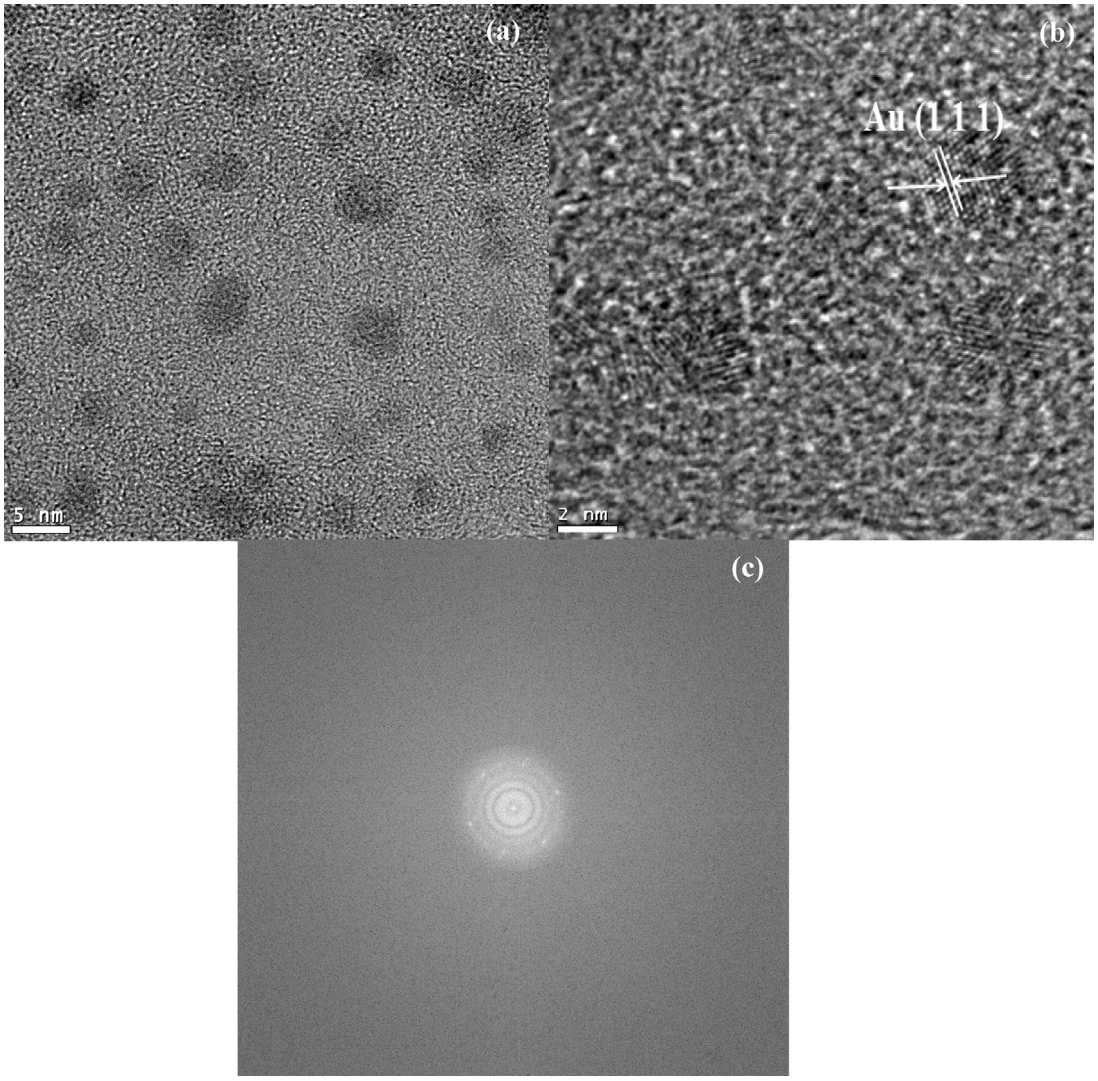

Fig. 3. Representative HRTEM ((a) and (b)) and FFT (c) images of gold nanoparticles.

Scherrer formula was ~21 nm which is in well accordance with the particle size calculated from the HRTEM studies.

Fig. 6a shows the Raman analysis of the TiO_2 and Au–TiO_2 nanocatalysts, the appearance of the Raman peaks at 639 cm^{-1} (E_g), 514 cm^{-1}(B_{1g}) and 395 cm^{-1} (A_{1g}) can be assigned to the anatase phase of titania [25]. Raman analysis of the pure gold nanoparticles cannot show any characteristic peaks or in other words the gold nanoparticles has not shown any response against the Raman spectral analysis. The raised hump (ca. ~420 cm^{-1}) in the Raman spectrum of Au–TiO_2 inspired us to find the reason for its formation. Nonetheless, the absence of the characteristic peaks at 323 and 346 cm^{-1} ruled out the possibility of Au—Cl bonding in the Au–TiO_2 nanocatalysts, similarly no other impurity is emanating a Raman response at ~420 cm^{-1}. To the best of our knowledge no such peak (ca. ~420 cm^{-1}) was reported in the literature for the Au–TiO_2 nanocatalysts. Therefore it needs some more analysis to confirm the context of the peak appeared in the Au–TiO_2 nanocatalysts. The comparison of the Raman spectrum of TiO_2 and Au–TiO_2 evidently shows the shift by ~5 cm^{-1} (Fig. 6b) at 639 cm^{-1} (E_g) for the corresponding nanophotocatalysts. The 639 cm^{-1} peak can be considered as the overtone of the Raman peak observed at 144 cm^{-1} for the single crystal TiO_2 anatase phase [26,27]. The observed shift at 639 cm^{-1} for the Au–TiO_2 nanocatalysts confirms the gold nanoparticles are loaded on the surface of TiO_2. Thus, the gold nanoparticles acts as a sink for the electronic charges produced during the photoexcitation. The delayed recombination of the electronic charges is expected to enhance the quantum yield of the Au–TiO_2 assisted catalytic processes [20–22].

The physicochemical characteristics of TiO_2 and Au–TiO_2 nanocatalysts were analyzed using BET analysis. The TiO_2 and Au–TiO_2 nanocatalysts show type IV adsorption–desorption isotherm during the analysis (Fig. 7). The loading of gold nanoparticles considerably changed the physicochemical characteristics of the resulting nanocatalysts as BET analysis (S_{BET}) of Au–TiO_2 shows an enhanced surface area (S_{BET} = 46 m^2/g) when compared with the bare TiO_2 (S_{BET} = 39 m^2/g). Similarly, pore volume (V_p) and other characteristics (Table 1) were rehabilitated in the resulting Au–TiO_2

Table 1
Physicochemical characteristics of TiO_2 and Au–TiO_2 nanophotocatalysts.

S. no.	Name of the nanocatalyst	S_{BET} (m^2/g)	V_p (cm^3/g)	V_o (cm^3/g)	V_m (cm^3/g)
1	TiO_2	39	0.06	0.02	0.04
2	Au–TiO_2	46	0.09	0.02	0.07

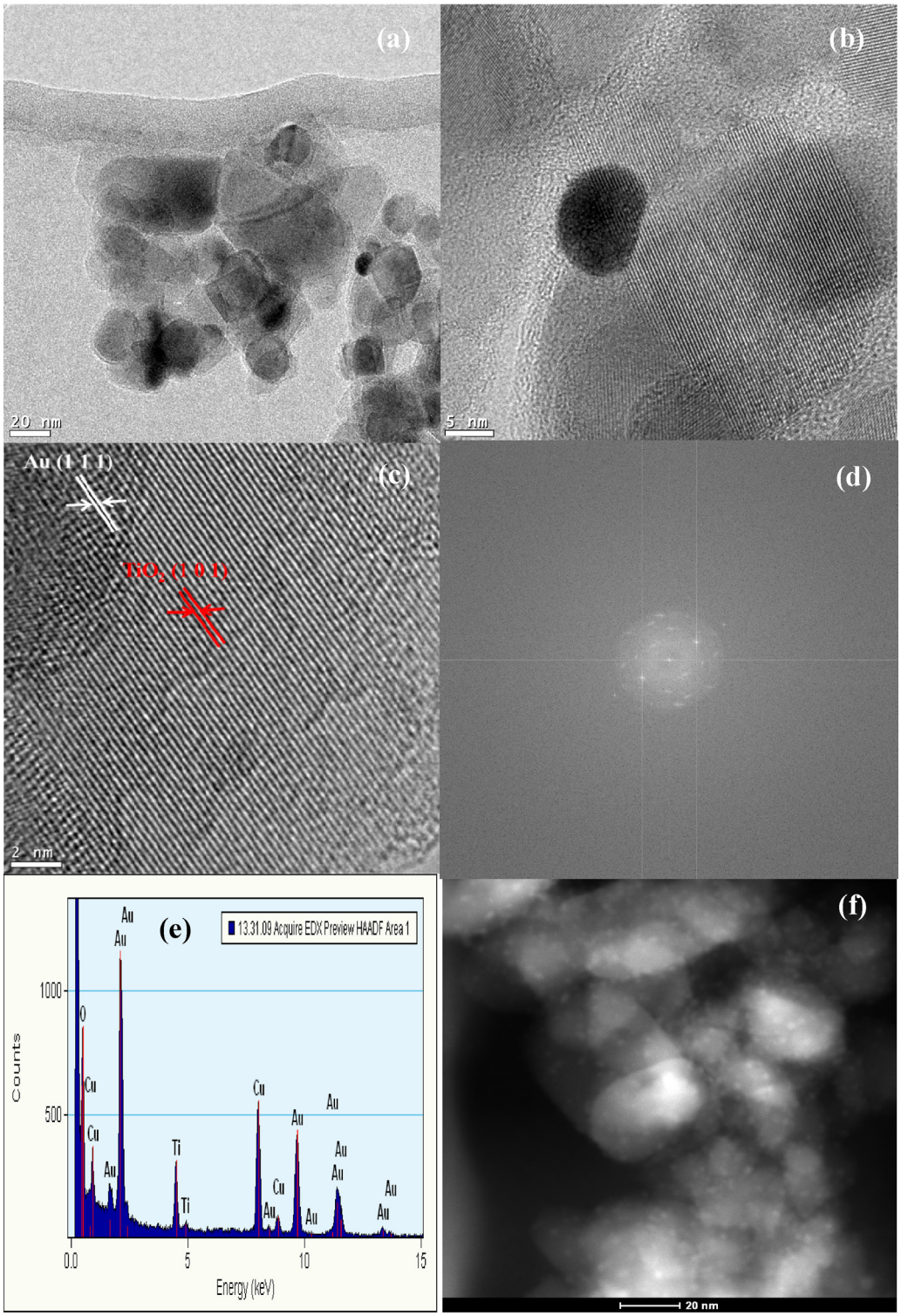

Fig. 4. HRTEM [(a) 10 nm, (b) 5 nm and (c) 2 nm] and FFT (d), EDAX (e) images of Au–TiO_2 nanocatalysts and the corresponding HAADF-STEM was shown in (f).

nanocatalysts. Fig. 8 shows diffuse reflectance (DR) UV–vis spectral analysis of TiO_2 and Au–TiO_2 nanocatalysts. The absorption band edge observed for the bare TiO_2 was ~390 nm which significantly indicates that the bare TiO_2 cannot be able to absorb the visible portion of the sun light. Nevertheless the Au–TiO_2 nanocatalysts conspicuously show the shift in the adsorption band edge (~420 nm) which gives the first notation that the Au–TiO_2 nanocatalysts can be utilized as the visible light responsive photocatalyst and the SPR peak observed at ~565 nm further confirms that the visible light is adequate to generate the electronic charges during the photocatalysis. The Tauc plot derived from Kubelka Munk Function (inset of Fig. 8) designates that the optical band gap of Au–TiO_2 was 2.6 eV whereas the bare TiO_2 shows 3.2 eV which endorses the visible light excitation of the Au–TiO_2 nanocatalysts.

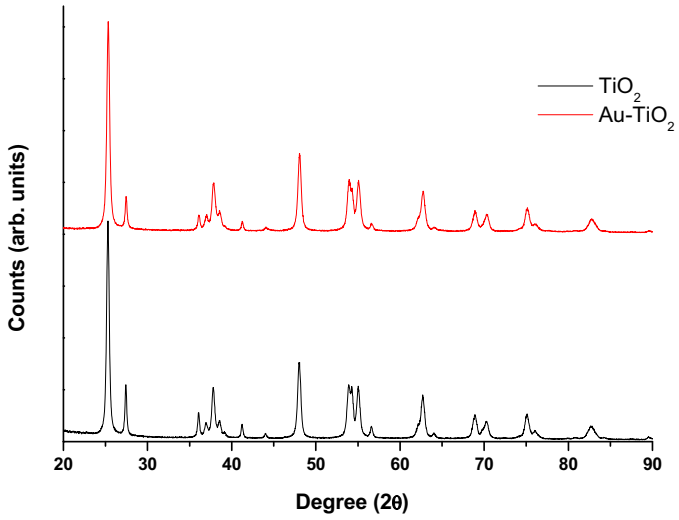

Fig. 5. XRD pattern of TiO_2 and Au–TiO_2.

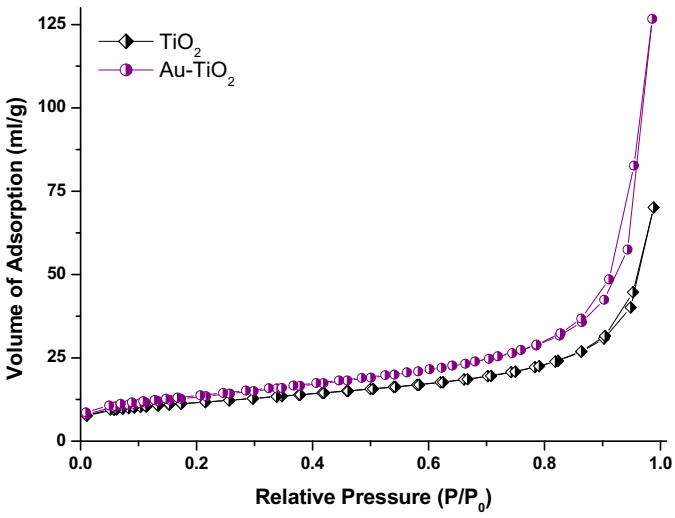

Fig. 7. BET analysis of TiO_2 and Au–TiO_2 nanophotocatalysts.

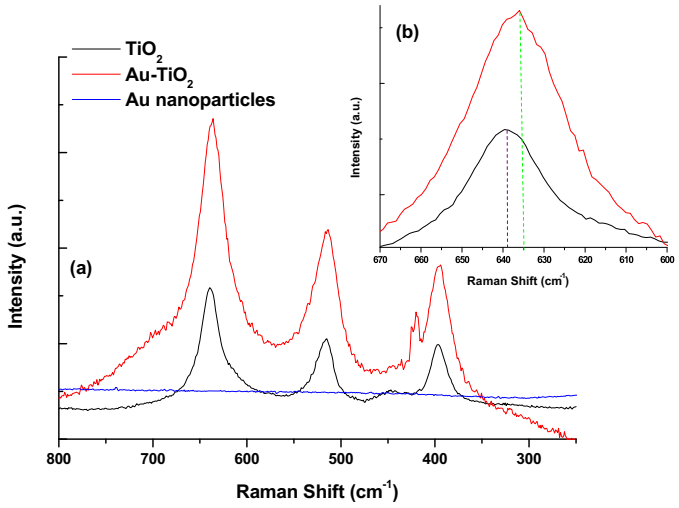

Fig. 6. Raman spectra of Au, TiO_2 and Au–TiO_2 nanophotocatalysts.

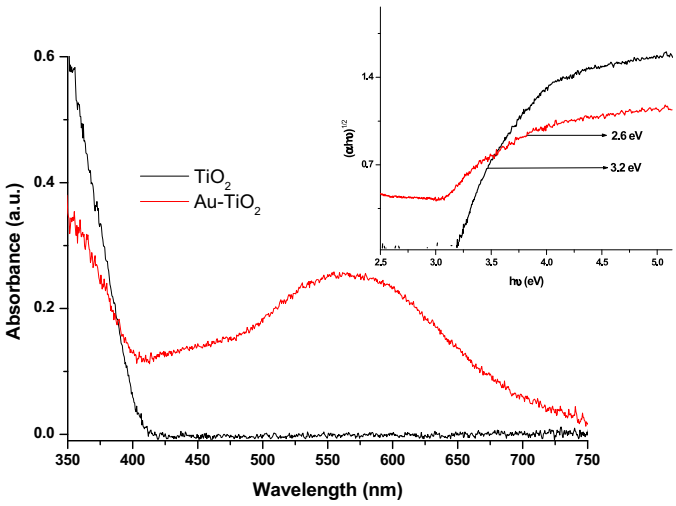

Fig. 8. Diffuse reflectance (DR)-UV–Vis spectra of TiO_2 and Au–TiO_2 nanophotocatalysts and the inset shows the Tauc plot derived from the Kubelka Munk Function for TiO_2 and Au–TiO_2.

3.2. Degradation of Simazine in the presence of Au–TiO_2 nanocatalysts

In this study, Simazine was taken as the model pollutant to examine the sonolytic, sonocatalytic, photocatalytic and sonophotocatalytic degradation in the presence of TiO_2 and Au–TiO_2 nanocatalysts. The initial concentration of Simazine was fixed at its maximum solubility (5 mg/L) for all the degradation processes. The concentration of the nanocatalysts was varied from 0.2 to 3 g/L in order to achieve the optimum concentration of the nanocatalyst which is required for the maximum degradation of Simazine. The kinetics of degradation was followed using a HPLC analyzer equipped with a PDA detector. A three dimensional representation of the HPLC chromatogram obtained during the sonophotocatalytic degradation of Simazine in the presence of Au–TiO_2 is shown in Fig. 9. The concentration of Simazine (RT = 2.5 min) was decreased with respect to the ultrasonic irradiation and the appearance of new peaks (RT = 1 to 2 min) can be identified from the HPLC chromatogram.

The sonolysis ($0.96 \times 10^{-4}\,s^{-1}$) and photolysis ($0.049 \times 10^{-4}\,s^{-1}$) of Simazine exhibit very low rate of degradation when compared with the rate achieved for the sonocatalytic ($1.61 \times 10^{-4}\,s^{-1}$), photocatalytic ($0.921 \times 10^{-4}\,s^{-1}$) and sonophotocatalytic degradation ($2.38 \times 10^{-4}\,s^{-1}$) of Simazine at the catalyst

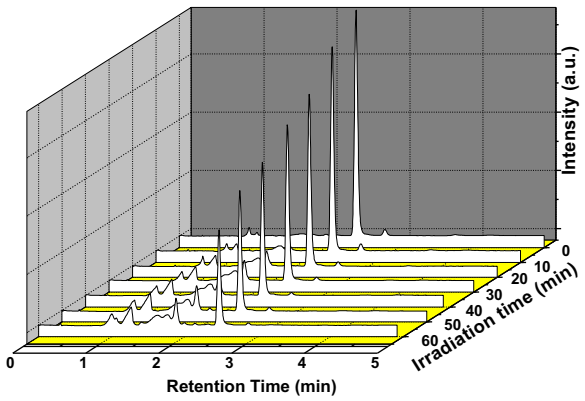

Fig. 9. 3-D plot showing the evolution of the HPLC chromatogram for the sonophotocatalytic degradation of Simazine at its fixed initial concentration 5 mg/L and [Au–TiO_2] = 1.5 g/L.

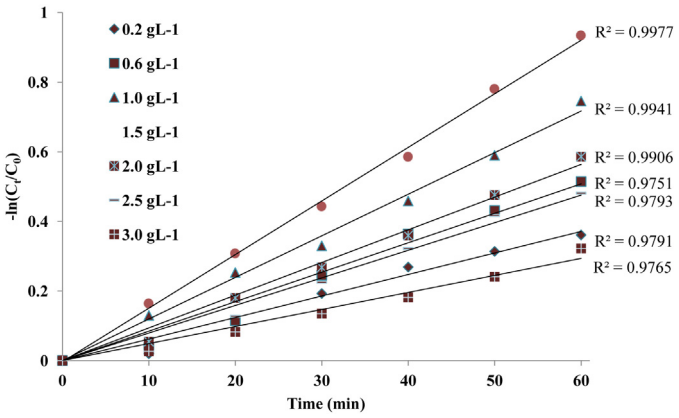

Fig. 10. Plot of variation of concentration of Au–TiO_2 up on irradiation time during sonophotocatalytic degradation of Simazine at its fixed initial concentration (5 mg/L).

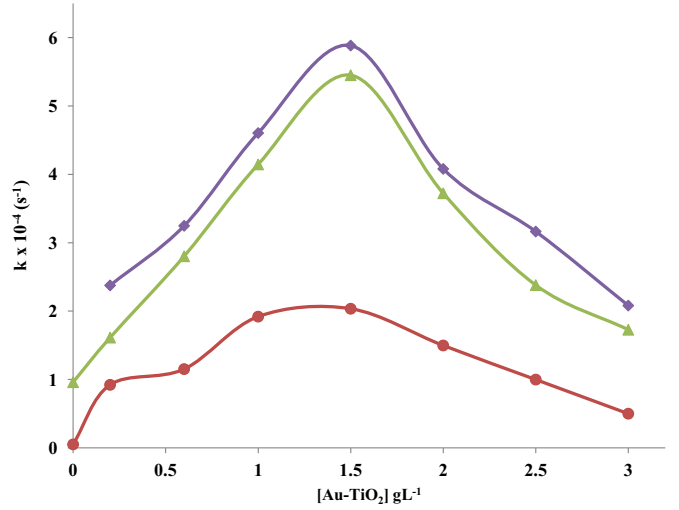

Fig. 11. Plot of rate constant vs [Au–TiO_2] for the sonophotocatalytic (♦), sonocatalytic (▲) and photocatalytic (●) degradation of Simazine.

dosage was 0.2 g/L (Au–TiO_2). This reveals that the degradation of Simazine needs a solid support to effectively interact with the hydroxyl radicals produced during the advanced oxidation process. Fig. 10 shows the $-\ln(C/C_0)$ vs time plot observed during the sonophotocatalytic degradation of Simazine in the presence of Au–TiO_2 at its various concentrations. The linear relationship between $-\ln(C/C_0)$ vs time indicates that the linear regression coefficient (R^2) was >0.97 for the sonophotocatalytic degradation of Simazine. Therefore, Simazine degradation can be considered to follow the first-order kinetics. The rate constants (k) observed for the various concentration of Au–TiO_2 for the degradation of Simazine during sonocatalytic, photocatalytic and sonophotocatalytic processes is depicted in Fig. 11. All the AOPs showed an increase in the rate constant with concentration of the nanocatalysts. The maximum sonocatalytic, photocatalytic and sonophotocatalytic degradation was achieved at 1.5 g/L. The nanocatalysts concentration [1.5 g/L] was fixed as the optimum concentration for the Simazine degradation. Further increase in the nanocatalysts concentration leads to decrease the efficiency of the process by reflecting the visible light entered into the photocatalytic microenvironment rather than the photo-initiation of electronic charges. On the other hand, it is observed from the Simazine degradation that the catalysis reactions experimented below the optimum nanocatalyst dosage needs more effective

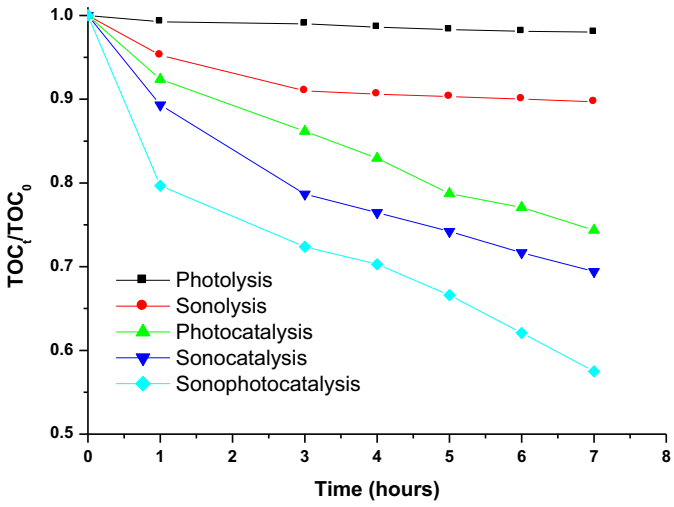

Fig. 12. Mineralization of Simazine (5 mg/L) during various advanced oxidation processes in the absence and presence of Au–TiO_2 (1.5 g/L) nanophotocatalysts.

surface area to achieve the enhanced rate of mineralization. The rate constants observed for the various AOPs assisted degradation of Simazine ($SC = 5.45 \times 10^{-4}\ s^{-1}$; $PC = 2.03 \times 10^{-4}\ s^{-1}$ and $SPC = 5.88 \times 10^{-4}\ s^{-1}$) revealed an enhanced rate of its degradation when compared with the rate constants observed in the presence of bare TiO_2 ($SC = 1.12 \times 10^{-4}\ s^{-1}$; $PC = 0.21 \times 10^{-4}\ s^{-1}$ and $SPC = 1.37 \times 10^{-4}\ s^{-1}$).

The application of ultrasound during the sonophotocatalytic process is not only creates the effective radicals which are required for the degradation process but also it continuously clean the surface of the nanocatalysts to avoid the accumulation of Simazine and its intermediates produced during the sonophotocatalysis. The combination of ultrasound irradiation and visible light enhances the production of the effective radicals needed for the degradation of Simazine nevertheless one such process is absent in the photocatalysis and sonocatalysis. However, sonophotocatalytic degradation exhibited an additive effect when the rate constants observed for the various AOPs are substituted in the following equation [28],

$$\text{Synergy} = \frac{k'_{\text{sonophotocatalysis}}}{k'_{\text{sonocatalysis}} + k'_{\text{photocatalysis}}}$$

The optimized nanophotocatalyst concentration (1.5 g/L) was employed for the sonocatalytic, photocatalytic and sonophotocatalytic mineralization of Simazine for the extended irradiation up to 7 h. Fig. 12 shows the visible light assisted photolysis alone cannot be able to initiate the mineralization of Simazine. The sonolysis of Simazine achieved 11% of the TOC removal from the initial concentration. However, the rate of mineralization attained during the photolysis and sonolysis are negligible when compared with the mineralization achieved for the sonocatalytic (31%), photocatalytic (26%) and sonophotocatalytic (43%) processes. The sonophotocatalytic degradation shows its greater applicability to the mineralization of Simazine since the direct band gap excitation and the utilization of ultrasound enhanced the number of effective radicals production which tends to attain the maximum rate of mineralization for Simazine. At the same time, the photocatalysis and sonocatalysis process demonstrates that the effective radicals production was decreased when the particular AOP was applied to the mineralization. On the other hand, mass transfer of the organic contaminants to the bulk solution was improved during the sonophotocatalytic degradation when compared with the sonocatalytic and photocatalytic degradation processes.

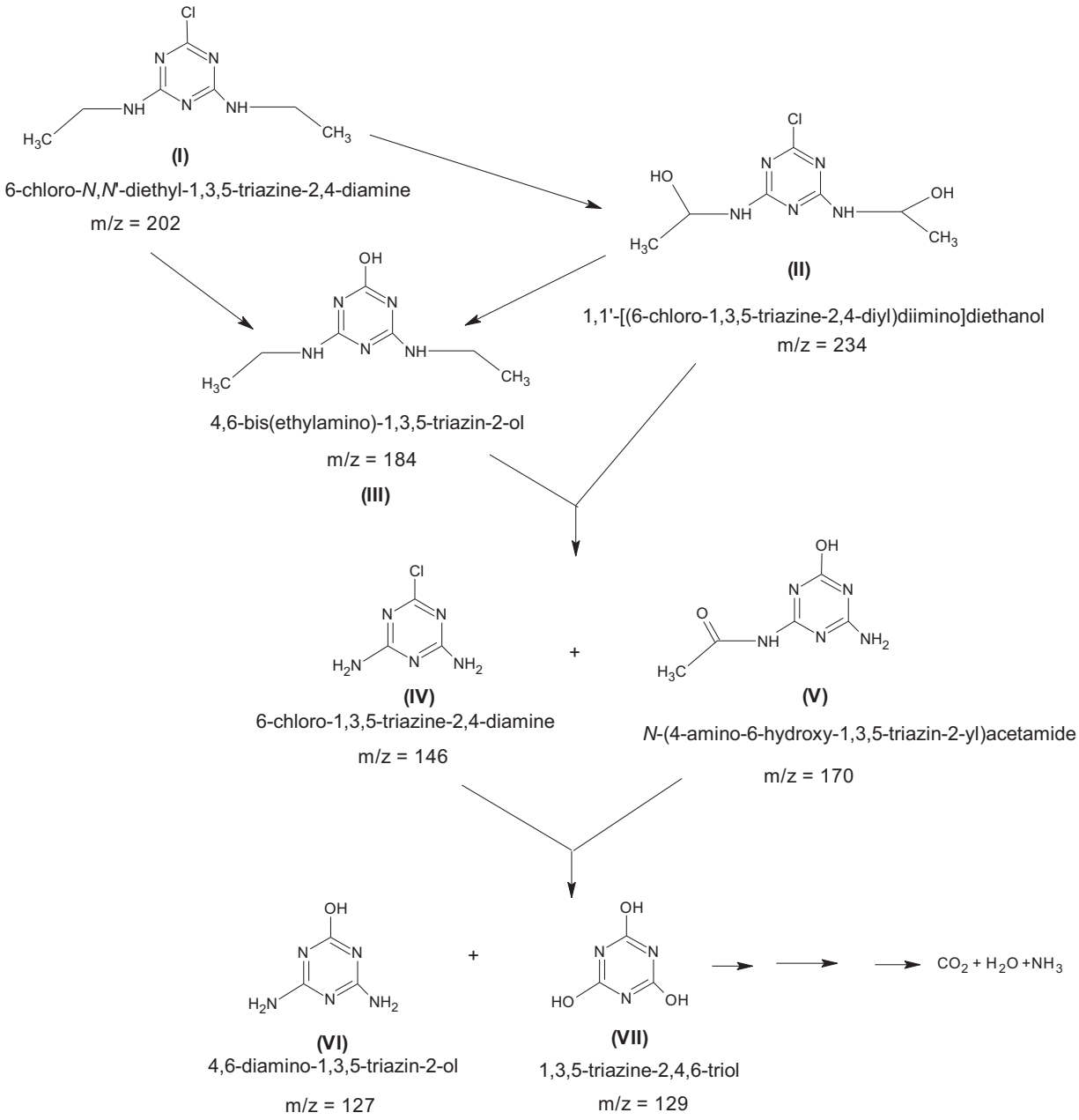

Scheme 1. Proposed pathway for the mineralization of Simazine during Au–TiO_2 assisted sonophotocatalysis.

The electro spray ionization mass spectrometry (ESI-MS) analysis was performed to identify the various intermediates produced during the sonophotocatalytic degradation of Simazine. The positive mode ESI-MS demonstrated that the various intermediates at $m/z = 234$, 184, 170, 146, 129 and 126 were produced during the mineralization. The ESI-MS analysis of the unprocessed solution clearly establishes the existence of Simazine (6-chloro-*N*,*N*′-diethyl-1,3,5-triazine-2,4-diamine) at $m/z = 202$ (I), thus ruled out the possibility of other impurities. The hydroxylated derivatives of Simazines are the major intermediates (II and III) identified from the ESI-MS analysis of the aliquots withdrawn from the sonophotocatalytically treated Simazine after 2 h. However, further sonophotocatalytic treatment of Simazine and hydroxylated Simazine lead to produce 6-chloro-1,3,5-triazine-2,4-diamine (IV) and *N*-(4-amino-6-hydroxy-1,3,5-triazin-2-yl)acetamide (V) as the intermediates and thus confirm the progress of further mineralization of Simazine. The aliquots withdrawn after 7 h of the sonophotocatalytic treatment showed that 4,6-diamino-1,3,5-triazin-2-ol (VI) and 1,3,5-triazine-2,4,6-triol (VII) are the major intermediates which clearly indicates that the triazine based skeleton cannot be easily mineralized. On the other hand, further sonophotocatalytic irradiation (>7 h) was expected to completely mineralize the Simazine and the various intermediates produced during its degradation into CO_2, H_2O and other small molecular products. Based on the identification of the intermediates observed from the sonophotocatalytic mineralization of Simazine in the presence of Au–TiO_2, and the available literature [11,29-31], we proposed a pathway for the Simazine degradation as shown in Scheme 1. The similar kind of pathway can be proposed for the photocatalytic and sonocatalytic degradation of Simazine. The identification of various intermediates was expected for the photocatalytic and sonocatalytic degradation apart from the intermediates observed for the sonophotocatalytic degradation.

4. Conclusion

The complete mineralization of Simazine by the low cost methodology was aimed in this study and it is demonstrated by using various advanced oxidation processes. To achieve the mineralization of Simazine, Au–TiO_2 nanophotocatalysts were synthesized using a commercial 42 kHz ultrasound producing bath type sonicator. The nanophotocatalysts were characterized using various analytic tools to confirm the existence of gold nanoparticles along with TiO_2. Significantly, Raman analysis confirms the existence of the gold nanoparticles on the surface TiO_2 which increased the visible light responsive nature of the Au–TiO_2 nanophotocatalysts. The Au–TiO_2 supported sonophotocatalysis of Simazine showed that 43% of the total organic carbon was removed from the Simazine after 7 h of the irradiation which enhances the possibility of using the electron acceptors for the rapid mineralization of large quantity of Simazine. The HPLC and ESI-MS analyses confirmed the concurrent and unselective decomposition of Simazine and its various degradation intermediates. The rapid development of such low cost methodologies for the mineralization of various organic contaminants significantly reduces the cost required for the advanced oxidation processes.

Acknowledgement

The authors would like to thank FONDECYT Postdoctorado project No.: 3120095 and FONDECYT no.: 1130916 Government of Chile, Santiago, for financial assistance.

References

[1] S. Navarro, J. Fenoll, N. Vela, E. Ruiz, G. Navarro, J. Hazard. Mater. 172 (2009) 1303–1310.
[2] A.S. Gunasekara, J. Troiano, K.S. Goh, R.S. Tjeerdema, Rev. Environ. Contam. Toxicol. 189 (2007) 1–23.
[3] N.H. Spliid, A. Helweg, K. Heinrichson, Chemosphere 65 (2006) 2223–2232.
[4] S. Devipriya, S. Yesodharan, Sol. Energy Mater. Sol. Cells 86 (2005) 309–348.
[5] H.D. Burrows, L.M. Canle, J.A. Santaballa, S. Steenken, J. Photochem. Photobiol. B: Biol. 67 (2002) 71–108.
[6] A. García-Valcárcel, J. Tadeo, J. Agric. Food Chem. 47 (1999) 3895–3900.
[7] L. Cox, R. Celis, M.C. Hermosin, J. Cornejo, J. Agric. Food Chem. 48 (2000) 93–99.
[8] J. Troiano, D. Weaver, J. Marade, F. Spurlock, M. Pepple, C. Nordmark, D. Bartkowiak, J. Environ. Qual. 30 (2001) 448–459.
[9] E.C. Catalkaya, F. Kargi, J. Hazard. Mater. 168 (2009) 688–694.
[10] M. Arias-Estévez, E. López-Periago, E. Martínez-Carballo, J. Simal-Gándara, J. Mejuto, L. García-Río, Agric. Ecosyst. Environ. 123 (2008) 247–260.
[11] M.J. López-Muñoz, J. Aguado, A. Revilla, Catal. Today 161 (2011) 153–162.
[12] C. Flores, V. Morgante, M. González, R. Navia, M. Seeger, Chemosphere 74 (2009) 1544–1549.
[13] F.J. Beltran, J.F. Garcia-Araya, V. Navarrete, F.J. Rivas, Ind. Eng. Chem. Res. 41 (2002) 1723–1732.
[14] F.J. Beltran, J.F. Garcia-Araya, J. Rivas, P.M. Alvarez, E. Rodriguez, J. Environ. Sci. Health B35 (2000) 439–454.
[15] T. Kodama, L.X. Ding, M. Yoshida, M. Yajima, J. Mol. Catal. B: Enzym. 11 (2001) 1073–1078.
[16] X. Chen, S.S. Mao, Chem. Rev. 107 (2007) 2891–2959.
[17] P. Sathishkumar, R.V. Mangalaraja, S. Anandan, M. Ashokkumar, Sep. Purif. Technol. 102 (2013) 67–74.
[18] P. Sathish Kumar, R. Sweena, J.J. Wu, S. Anandan, Chem. Eng. J. 171 (2011) 136–140.
[19] S. Anandan, P. Sathish Kumar, N. Pugazhenthiran, J. Madhavan, P. Maruthamuthu, Sol. Energy Mater. Sol. Cells 92 (2008) 929–937.
[20] V. Subramanian, E. Wolf, P.V. Kamat, J. Am. Chem. Soc. 126 (2004) 4943–4950.
[21] V. Subramanian, E. Wolf, P.V. Kamat, J. Phys. Chem. B105 (2001) 11439–11446.
[22] N. Fuke, A. Fukui, A. Islam, R. Komiy, R. Yamanaka, H. Harima, L. Han, Sol. Energy Mater. Sol. Cells 93 (2009) 720–724.
[23] S. Anandan, M. Ashokkumar, Ultrason. Sonochem. 16 (2009) 316–320.
[24] P. Sathish Kumar, A. Manivel, S. Anandan, M. Zhou, F. Grieser, M. Ashokkumar, Colloids Surf., A: Physicochem. Eng. Aspects 356 (2010) 140–144.
[25] R.A. Naphade, M. Tathavadekar, J.P. Jog, S. Agarkar, S. Ogale, J. Mater. Chem. A 2 (2014) 975–984.
[26] Y.L. Du, Y. Deng, M.S. Zhang, J. Phys. Chem. Solids 67 (2006) 2405–2408.
[27] Y. Li, H. Wang, Q. Feng, G. Zhou, Z. Wang, Energy Environ. Sci. 6 (2013) 2156–2165.
[28] P. Sathishkumar, R.V. Mangalaraja, O. Rozas, H.D. Mansilla, M.A. Gracia-Pinilla, S. Anandan, Ultrason. Sonochem. 21 (2014) 1675–1681.
[29] V. Morgante, C. Flores, X. Fadic, M. González, M. Hernández, F. Cereceda-Balic, M. Seeger, J. Environ. Manage. 95 (2012) S300–S305.
[30] W. Chu, Y. Rao, W.Y. Hui, J. Agric. Food Chem. 57 (2009) 6944–6949.
[31] Y. Rao, W. Chu, Ind. Eng. Chem. Res. 52 (2013) 13580–13586.